Operation of Three-Phase Resonant Converter in Single-Phase AC-to-DC Applications

*H. M. Suryawanshi[1], S. S. Tanavade[2], K. L. Thakre[3] and M. A. Chaudhari[4]

Abstract – **A single-phase ac-to-dc converter using three-phase modified series-parallel resonant converter is proposed in this paper. The three-phase resonant converter is analyzed using Fourier series approach. The design curves for a resonant converter of 2.5 kW rating are plotted. The converter components are selected based on the design curves. The converter is simulated for different load conditions using PSIM. A laboratory prototype of the converter is built. It is operated at 290 kHz on full load condition. The variable frequency control is implemented using digital signal processor for the output voltage regulation. The converter performance is verified using the simulation and experimental results. The use of three-phase high frequency inverter reduces the filtering requirements, peak component stresses on the resonant components and peak inverter output current. The proposed converter maintains excellent input line power factor without any active control of ac input line current. Apart from this, it requires narrow variation in switching frequency for its output voltage regulation.**

Keywords - Three-phase resonant converter, high power factor, high frequency operation, ZVS operation

List of Symbols

N	=	Number of turns
M	=	Normalised converter gain
J	=	Normalised load current
ω_s	=	Switching frequency (radian/sec)
ω_r	=	Resonant frequency (radian/sec)
ρ_c	=	Resistivity of copper
b_c	=	Breadth of window area of the core
k_F	=	Factor accounting for field distribution
b_b	=	Breadth of bobbin
h	=	Height allocated for winding
F_p	=	Turn packing factor for turns in the winding relative to perfect square packing
d_r	=	Diameter of 40 AWG wire
F_{lp}	=	Factor accounting for serving area, bundle pack, strand packing and effect of twist on diameter
α, β	=	Constants with values 1.12 and 0.97 respectively
C_n	=	Snubber capacitor

I. INTRODUCTION

The demand for isolated DC power with high power-packing density is ever increasing. Single-phase resonant converters are being used popularly in such small power tank circuits face severe voltage as well as current stresses. applications. For high power requirements, the components in the single-phase resonant Hence the resonant converters using three-phase tank circuits are becoming increasingly popular [1-11]. A. R. Prasad proposes [2] a three-phase parallel resonant dc-to-dc converter using fixed frequency PWM technique for isolated dc power supply applications. It is shown that the combination of resonant and PWM control methods can be used to tightly regulate the output voltage from no-load to full-load at constant switching frequency and with low switching losses. Moreover it is also shown that this converter exhibits significantly lower current stresses in resonant inductor, inverter switches and the resonant capacitor. A. K. S. Bhat demonstrates [5-6] an LCC type three-phase resonant converter used in a dc-to-dc conversion, in which all the switches operate in ZVS for the complete load range under variable frequency control. It has also been shown that the switch peak currents decrease with the load current. In a direct comparison of this converter with a single-phase same rated LCC resonant converter, it has been shown that the peak current as well as voltage stresses on the resonant tank components are much lower in the three-phase converter. Thus the three-phase resonant converters have many advantages over the single-phase resonant converters.

In this paper a single-phase ac-to-dc converter using three-phase modified series-parallel resonant converter (MSPRC) for input line power factor improvement is presented. Advantages of Modified series-parallel resonant converter are well known [12-13]. The converter is analyzed using Fourier series approach. Design curves for the converter are plotted to select the optimum value for the quality factor. The converter components for its optimum performance are selected using a step-by-step design procedure. The designs for the magnetic components and Litz wire are also discussed. A laboratory prototype of the converter is built for 2.5 kW rating. It is operated at minimum switching frequency of 290 kHz (on full load condition) to increase power-packing density. Since the power factor depends upon the ratio of switching frequency to the resonant frequency, the operation at higher switching frequency also results in the high power factor at the ac input line. Variable frequency control is implemented using a digital signal processor for the output voltage regulation. This converter maintains high input line power factor without any active control of input line current throughout the load range. It is shown that under varying load conditions, the converter operates in ZVS mode and requires a narrow variation in switching frequency for its output voltage regulation. Such a converter is useful in the sophisticated electrical drives and high power dc supplies.
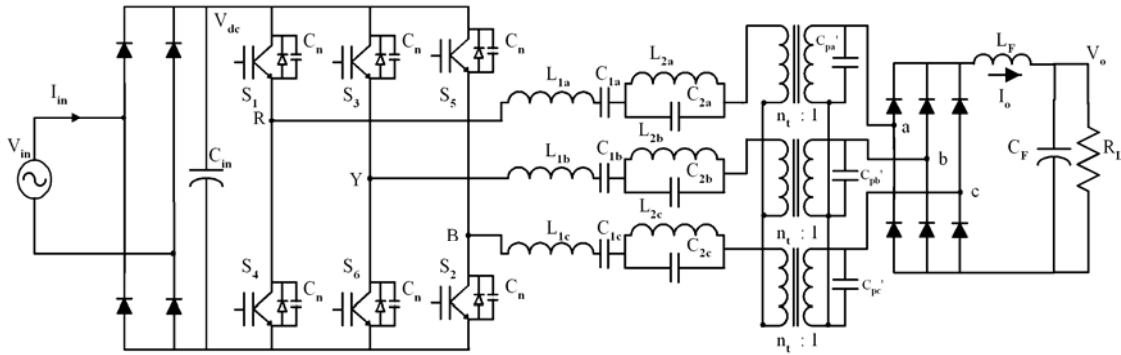
Fig. 1: The AC to DC converter using three-phase modified series-parallel resonant converter.

The major contribution of the paper includes the analysis using Fourier approach and design of three-phase HF resonant converter in single-phase AC-to-DC applications. The features of three-phase resonant inverter over single-phase resonant inverter: better utilization of HF transformer core, high power transfer for the same switch current, lower losses and component stresses owing to lower average switch current for the same power level and reduced HF output ripple allowing smaller size filter elements. High efficiency is achieved due to reduction in losses by zero-voltage switching (ZVS), and pure sinusoidal current flow through the switching devices because of resonant tank circuit. It also contributes to the design of litz wire for minimizing the eddy current loss due to skin effect.

II. OPERATING PRINCIPLE AND ANALYSIS

The proposed ac-to-dc resonant converter that employs the three-phase modified series-parallel resonant tank circuit with output LC filter is shown in Fig. 1. To regulate the output voltage of the converter variable frequency control with 1800 wide gating pulses scheme is used. The converter switching frequency is kept above the resonant frequency of the tank circuit. This scheme maintains the lagging power factor resulting in zero voltage switching (ZVS) of the HF inverter switches. Due to ZVS operation throughout the load range, the turn-on losses are practically eliminated. The turn-off losses are reduced by connecting loss-less capacitive snubbers across the HF switches. This results in higher efficiency over the entire load range. Moreover, since the converter operates above resonance frequency, the output filter can be designed for the full load operating frequency. Reactive components of the modified series-parallel resonant tank circuit in each phase of the three-phase HF inverter include L1, L2, C1, C2 and Cp′. The capacitor Cp′ is connected across the secondary of HF transformer to achieve advantages of its leakage reactance referred to primary. This reduces the actual value of resonant inductor externally needed in the tank circuit.

Quasi-square wave voltages of HF inverter drive the three-phase tank circuit. Three-phase HF transformer (Y-Y) is used for isolation as well as voltage transformation.

Output voltage of HF transformer is rectified using three-phase HF diode Bridge to obtain dc output voltage. The output filter components L_F and C_F are designed at full

load condition for the specified current and voltage ripple contents in the output respectively.
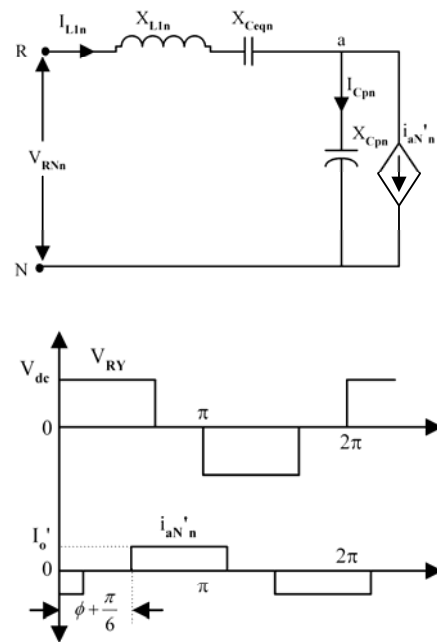

Fig. 2 (a) Per-phase equivalent circuit model for the nth harmonic of the three-phase MSPRC. (b) Per-phase waveforms of the converter

The proposed converter is analyzed using Fourier series analysis. To obtain a simplified model for this purpose, all the components on the secondary side of the HF transformer are referred to its primary. Further the rectifier input current of each phase is assumed to be a quasi-square wave of amplitude $I_o′$. The per-phase equivalent circuit and the waveforms using constant current model are shown in Fig. 2. For normalizing the equations in this section, following base values are chosen for voltage, impedance and current respectively.

$$V_B = V_{dc}, \ Z_B = \sqrt{L_1/C_{eq}}, \ I_B = V_B/Z_B \tag{1}$$

where, $C_{eq} = \dfrac{C_1}{1+\alpha}$, $\alpha = \dfrac{C_1/C_2}{\left[1 - \left(1/y^2\omega_r^2 L_2 C_2\right)\right]}$, $y = \dfrac{\omega_s}{\omega_r}$

All the normalized quantities are denoted by an additional

subscript 'o'. Using this notation, the normalized reactances for n^{th} harmonic referred to Fig. 2 (a) are,

$$X_{L1no} = \frac{n X_{L1}}{Z_B} = ny$$

$$X_{Ceqno} = \frac{X_{Ceq}/n}{Z_B} = \frac{1}{ny}$$

$$X_{CPno} = \frac{X_{Cp}/n}{Z_B} = \frac{1}{ny} \cdot \frac{C_{eq}}{C_p} \qquad (2)$$

$$X_{seriesno} = X_{L1no} - X_{Ceqno} = \frac{n^2 y^2 - 1}{ny}$$

$$X_{eqno} = X_{seriesno} - X_{Cpno}$$

The resonant frequency $\omega_r = \dfrac{u}{\sqrt{L_1 C_1}}$ $\qquad (3)$

Where,

$$u = \sqrt{a\left(a\,s + \sqrt{a^2 s^2 - 4}\right)/2},$$

$$a = \sqrt{pq}, \; s = 1 + \frac{1}{p} + \frac{1}{pq}, \; p = \frac{L_1}{L_2}, \; q = \frac{C_1}{C_2}, \; r = \frac{C_1}{C_p}$$

The converter gain is given by, $M = V_o'/V_{in}$ where,

$V_o' = n_t V_o$

The normalized load current $J = I_o'/I_B$ where,

$I_o' = I_o/n_t$

The expressions for normalized line-to-line quasi-square wave voltage V_{RYno} and normalized line-to-neutral voltage V_{RNno} are as below.

$$V_{RYno} = \frac{4}{\pi} \sum_{n=6 \cdot k \pm 1}^{\infty} \frac{1}{n} \sin(n\omega_s t + n\pi/6) \cos(n\pi/6) \qquad (4)$$

$$V_{RNno} = \frac{2}{\pi} \sum_{n=6 \cdot k \pm 1}^{\infty} \frac{1}{n} \sin(n\omega_s t) \qquad (5)$$

The expressions for the other two phases can be obtained by phase shifting the above equations by 120^0 and 240^0 respectively. The rectifier input current of phase R referred to primary side is represented by,

$$i_{aN}{}'_{no} = \frac{4J}{\pi} \sum_{n=6 \cdot k \pm 1}^{\infty} \frac{1}{n} \sin(n\omega_s t - n\phi) \cos(n\pi/6) \qquad (6)$$

Referring to the Fig. 2 (a) following equations are written.

$$V_{RNno} = I_{L1no} X_{seriesno} + I_{Cpno}\left(-X_{Cpno}\right) \qquad (7)$$

$$i_{aN}{}'_{no} = I_{L1no} - I_{Cpno} \qquad (8)$$

Substituting I_{Cpno} from equation (8) into equation (7) and simplifying it, the normalized instantaneous current through the resonant tank circuit is,

$$I_{L1no} = \sum_{n=6 \cdot k \pm 1}^{\infty} \sqrt{a_n^2 + b_n^2} \cdot \sin(n\omega_s t + \theta_n) \qquad (9)$$

where, $a_n = \dfrac{4J(\sin n\phi)(\cos n\pi/6) X_{Cpno}}{n\pi X_{eqno}}$

$$b_n = \frac{2\left(1 - 2J(\sin n\phi)(\cos n\pi/6) X_{Cpno}\right)}{n\pi X_{eqno}}$$

$$\theta_n = \tan^{-1} \frac{b_n}{a_n}$$

Using equation (9), the expressions for the normalized instantaneous voltages across resonant tank components are written as follows.

$$V_{L1no} = I_{L1no} X_{L1no} = \sum_{n=6 \cdot k \pm 1}^{\infty} \sqrt{c_n^2 + d_n^2} \cdot \sin(n\omega_s t + \gamma_n) \quad (10)$$

$$V_{C1no} = I_{L1no} X_{C1no} = \sum_{n=6 \cdot k \pm 1}^{\infty} \sqrt{e_n^2 + f_n^2} \cdot \sin(n\omega_s t + \xi_n) \quad (11)$$

$$V_{C2no} = V_{L2no} = I_{L1no} X_{C_{C2L2 no}}$$

$$= \sum_{n=6 \cdot k \pm 1}^{\infty} \sqrt{l_n^2 + m_n^2} \cdot \sin(n\omega_s t + \eta_n) \qquad (12)$$

$$V_{Cpno} = V_{aN}{}'_{no} = V_{RNno} - I_{L1no} X_{seriesno}$$

$$= \sum_{n=6 \cdot k \pm 1}^{\infty} \sqrt{g_n^2 + h_n^2} \cdot \sin(n\omega_s t + \psi_n) \qquad (13)$$

where, $c_n = b_n X_{L1no}$, $d_n = a_n X_{L1no}$, $\gamma_n = \tan^{-1} \dfrac{c_n}{d_n}$

$e_n = b_n X_{C1no}$, $f_n = a_n X_{C1no}$, $\xi_n = \tan^{-1} \dfrac{e_n}{f_n}$

$l_n = b_n X_{C_{C2L2 no}}$, $m_n = a_n X_{C_{C2L2 no}}$, $\eta_n = \tan^{-1} \dfrac{l_n}{m_n}$

$g_n = \dfrac{2}{n\pi} - b_n X_{seriesno}$, $h_n = -a_n X_{seriesno}$, $\psi_n = \tan^{-1} \dfrac{g_n}{h_n}$

$X_{C_{C2L2}}$ = equivalent reactance of parallel combination of X_{L2} and X_{C2}.

For evaluating the above equations, the angle ϕ between $i_{aN}{}'_{no}$ and V_{RNn} must be known. This can be determined numerically by using the condition that $i_{aN}{}'_{no}$ starts flowing in the positive direction when $V_{aNn} = V_{cNn}$. The normalized converter gain M is given by,

$$M = \frac{V_o{}'_o}{V_{ino}} = \frac{6\sqrt{2}}{\pi^2} \int_{\phi + \frac{\pi}{6}}^{\phi + 5 \cdot \frac{\pi}{6}} V_{aN}{}'_{no} \cdot d\omega_s t \qquad (14)$$

III. DESIGN OF CONVERTER

Owing to the filtering action of resonant tank circuit, the fundamental component of the inverter output current is much larger than the harmonics. Hence for the design procedure of the converter in this section, the sine wave approximation is considered for the voltage and the current waveforms. Further, the higher switching frequency is chosen at full load condition results in high input power factor, since the power factor depends upon the ratio of the switching frequency to resonant frequency.

Input voltage, V_{in} = 230 V (rms), f_{in} = 50 Hz

Output voltage, V_o = 250 V

Output power, P_o = 2.5 kW

Resonant frequency, f_r = 282 kHz

Minimum switching frequency, f_s = 290 kHz

Peak to peak output current ripple, I_{p-p} = ±5 % of I_o

Peak to peak output voltage ripple, V_{p-p} = ±10 % of V_o

For near optimum values of converter gain, total kVA per kW rating of the resonant tank circuit and the inverter output current, the following inductor and capacitor ratios are selected [12].

$$\frac{L_1}{L_2} = 0.1, \quad \frac{C_1}{C_2} = 0.1, \quad \frac{C_1}{C_p} = 10$$

For the above inductor and capacitor ratios, the design curves as shown in Fig. 3 are plotted for various values of Q, using program developed in MATLAB. From Fig. 3, it can be seen that for near optimum values of converter gain, kVA rating of the resonant tank circuit per kW output of the converter, peak inverter output current and switching frequency variation for output voltage regulation the value of 1.8 is selected for Q.

Using equation (5), the rms value of the fundamental component of the line-to-neutral voltage of the HF inverter equals 93.18 V. Considering the design of resonant converter at resonant frequency, the tank gain is approximately unity. Thus from Fig.1, the voltage across primary winding of HF transformer is 93.18 V. To obtain 250 V dc output voltage, the phase voltage of 106.87 V is needed at the input terminals of three-phase HF diode bridge rectifier. Hence the transformation ratio n_t for the HF transformer is 93.18:106.87 $\cong$ 0.87:1. The quality factor Q of resonant tank circuit is given by,

$$Q = \frac{\omega_r L_1}{R'_L} \tag{15}$$

Using equations (3) and (15), the optimum component values for the tank components are calculated as given below.

L_1 = 19.22 μH, L_2 = 192.2 μH, C_1 = 0.0182 μF, C_2 = 0.182 μF, C_p = 0.00182 μF, $C_p' = n_t^2 C_p$ = 0.00138 μF

A. Design of magnetic components and litz wire

Magnetic components of the converter shown in Fig.1 (inductors L_1 and L_2 in the tank circuit, HF transformer and the filter inductance L_F) need to be designed to minimize the core and the winding losses. Since ferrite materials provide very high specific resistance, the eddy current losses in the core made-up of these materials may be practically disregarded. Ferrite materials M33 (frequency range 200 kHz to 1.6 MHz) and N87 (frequency range up to 500 kHz) of Siemens make find their usage in high Q inductors in the resonant circuits and transformers respectively. Hence for L_1 and L_2, pot cores P26x16 made-up of M33 material while for the HF transformer E30x15x7 cores made-up of N87 material are used. Further to 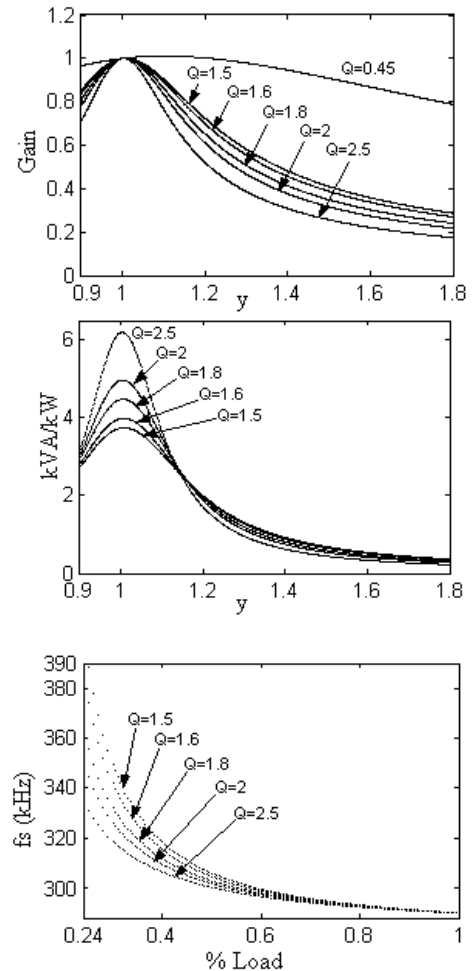minimize the winding losses due to skin effect, Litz wires (conductors made-up of multiple, individually insulated strands twisted together) are used for the winding of the inductors and the HF transformer.

For the given number of turns and winding cross sectional area, as the number of strands in a litz wire is increased, cross sectional area of each strand must be decreased. This typically leads to reduction in eddy current loss. However, as the number of strands increase, the fraction of window area filled with copper decreases and the fraction filled with the insulation increases. This results in increased dc resistance. Eventually, eddy current loss is made small till increasing dc resistance offsets any further improvement in it. Thus there is an optimal number of strands n_{opt}, that results in minimum winding loss [14, 15]. This is given by,

$$n_{opt} = \left[\left(\frac{2}{\beta} - 1 \right) \cdot \gamma \middle/ \left(\frac{1}{\beta} - 1 \right) \right]^{\frac{1}{\left(\frac{3}{\beta} - 2 \right)}} \tag{16}$$

where,

$$\gamma = \frac{\pi^2 \cdot N^2 \cdot \omega_s^2 \cdot \mu_0^2 \cdot d_r^{\left(6 - \frac{6}{\beta}\right)} \cdot \alpha^{-\frac{6}{\beta}} \cdot \left(F_p \cdot F_{lp} \cdot b_b \cdot \frac{h}{N} \right)^{\frac{3}{\beta}} \cdot k_F}{768 \cdot \rho_c^2 \cdot b_c^2}$$
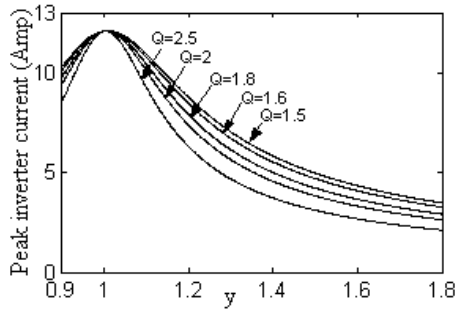

84

Fig. 3: Converter design curves for $L_1/L_2 = 0.1$, $C_1/C_2 = 0.1$ and $C_1/C_p = 10$. (a) Converter gain (b) kVA per kW for tank circuit (c) Switching frequency variation for output voltage regulation and (d) Peak inverter output current.

This will give non-integral number of strands, the nearest integral number of strands can be chosen to minimize ac resistance and hence to minimize the winding loss. The calculations for optimum number of strands for L_1 are done using equation (16) for minimum winding loss. These calculations suggest the use of 2136 strands of 52 AWG wire for L_1. AC resistance factor (F_{ac}), dc resistance factor (F_{dc}) and the total resistance factor (F_r) that is a product of F_{ac} and F_{dc} are plotted as a function of number of strands in Fig. 4. Fig. 4 reveals that a decrease from optimum of 2136 strands to 260 strands entails only a small increase in ac resistance (from 2.002 to 2.351) and hence in losses. However this results in a cost effective design. Thus cost trade-off becomes necessary. A MATLAB program is developed to find the variation in total resistance factor and relative cost for the optimal as well as sub-optimal strands for L1. This is shown in Table 1. Cost of the design with 44 AWG wire is taken as reference. To have best cost-loss compromise, the design with 260 strands of 42 AWG is selected for inductance L1. Similar design procedure is used to design inductance L2. To design the HF transformer of the ratio nt = 0.87 on EE 30x15x7, N87 ferrite core, 10 and 12 turns on primary and secondary are wound. Table 2 shows the different designs for the HF transformer. Although the design 'D7' with 48 AWG wire results in minimum loss, its relative cost is high. Hence to have cost-loss trade-off, the design 'D4' with 42 AWG wire is selected that gives slightly higher loss with lesser relative cost.

B. Output filter design

The output filter inductance L_F must suppress the switching frequency component of rectified resonant capacitor voltage V_r. This component has a minimum ripple frequency of 1.74 MHz (six times the inverter switching frequency). The magnitudes of its harmonic components are given by,

$$V_{rn} = \frac{2V_o}{4n^2 - 1} \tag{17}$$

where n is in multiples of $2f_s$. The dominant component of this voltage is at $n = 3$ i.e. at $6f_s$. This is given as,

$$V_{r3} = \frac{2V_o}{35}$$

The value of filter inductance is calculated using the peak-to-peak ripple specification of output current as below.

$$L_F = \frac{2(2V_o/35)}{6\omega_s I_{p-p}} = \frac{V_o}{105\pi f_s I_{p-p}} \tag{18}$$

The magnitudes of the harmonic components of the rectified output current are given by,

$$I_{rn} = \frac{2 I_o}{4 n^2 - 1} \tag{19}$$

The dominant component of this current is at $n = 1$ i.e. at $2 f_{in}$.

This is given by, $I_{r1} = \frac{2 I_o}{3}$

The output filter capacitance C_F, which is required to limit the double line frequency component of the rectifier output voltage to the ripple specification V_{p-p} is determined
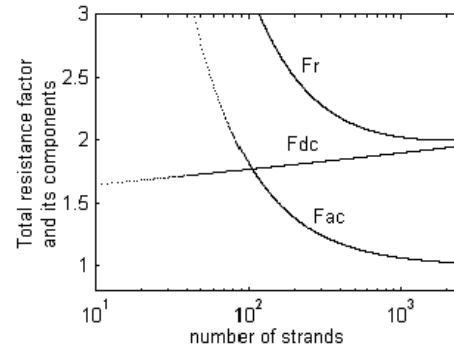
F_r is total resistance factor; F_{dc} and F_{ac} are dc and ac resistance factors

Fig. 4: Variation of resistance factors with strands for a Litz wire wound inductor (L_1)

Table 1: Design table for L_1 for optimal and sub-optimal stranding.

AWG	Strands	Fr	Relative Cost
38	70	3.886	0.33
39	100	3.231	0.36
40	175	2.607	0.49
41	225	2.431	0.55
42	**260**	**2.351**	**0.57**
44	485	2.132	1
52	2136	2.002	51.42

Table 2: Winding design table for HF transformer.

Design	Gauge W_1	Gauge W_2	Strands W_1	Strands W_2	Relative Cost	Relative Loss
D1	38	38	70	70	0.29	1.95
D2	40	40	175	175	0.51	1.54
D3	41	41	225	225	0.57	1.36
D4	**42**	**42**	**260**	**260**	**0.59**	**1.24**
D5	44	44	485	485	1	1
D6	46	46	972	972	2.65	0.97
D7	48	48	1524	1524	7.35	0.69
D8	50	50	1932	1932	20.38	0.72
D9	52	52	2136	2136	53.55	0.95

using the equation (20) given as

$$C_F = \frac{2(2 I_o/3)}{2 \omega_{in} V_{p-p}} = \frac{I_o}{3 \pi f_{in} V_{p-p}} \tag{20}$$

The use of L_F reduces the charging current of C_F. This in turn reduces the line current of the inverter, improving the efficiency of converter. This also reduces the stresses on the resonant tank components. The filter inductance L_F is

designed to suppress the switching frequency ripple in the output current. This ripple frequency is six times the switching frequency (1.74 MHz at full load for switching frequency of 290 kHz). Thus, the filtering requirements are drastically reduced. The values of L_F and C_F calculated using equations (18) and (20) are 2.61 μH and 424 μF respectively.

IV. EXPERIMENTAL RESULTS

The converter designed in section 3 is simulated using PSIM. The behavior of the converter at different load conditions is studied. Fig. 5 shows the results of ac input line voltage and line current at full load condition, at 50 % and 25 % of full load condition. The converter maintains high input line power factor for the entire load range. The inverter switches operate in ZVS mode.

The single-phase ac-to-dc converter using three-phase MSPRC, designed in section 3, is built to verify its performance. The actual components used for experimentation are as follows. The IGBT-HGTG20N60A4D, HF diodes DSEI 60-12A, L1= 19.25 μH including 1.66 μH leakage inductance of HF transformer, L2 = 190 μH, C1 = 0.02 μF, C2 = 0.2 μF, Cp´ = 1500 pF, LF = 2.61 μH, CF = 440 μF, load resistance at full load 25 Ω. A small EMI filter as shown in Fig. 6 is used at the input to suppress the high frequency switching noise and ripple.

To regulate the output voltage of this converter, the variable frequency control scheme is implemented using a digital signal processor (DSP) TMS320LF2812. The use of DSP facilitates the accurate generation of gating pulses for the HF inverter switches with the minimal hardware requirement. The insertion of equal and precisely calculated dead bands between the switching instants of the devices in all the three HF inverter legs is an easy task using the inbuilt programmable dead band units of the DSP. Moreover, along with the output voltage regulation, the functions like overload protection, analog to digital conversion of various analog parameters used for converter control, digital filtering of these sensed parameters and PID control algorithm are also implementable using the software techniques. At high switching frequencies transistorized gate driver circuits are insufficient to drive IGBTs. Further to achieve good performance and to avoid false triggering of the IGBTs during their off state, bipolar gate drivers are needed. Hence a high performance bipolar gate driver scheme using high speed MOSFETs (IRF510 and IRF9510) is fabricated for driving three-phase HF inverter.

The inductors L1 and L2 in the resonant tank circuit are wound on P26x16, M33 ferrite cores using 260/42 AWG (260 strands made-up of 42 AWG wire) and 100/42 AWG (100 strands made-up of 42 AWG wire) litz wires respectively. Use of M33 ferrite cores and litz wires greatly reduced the core losses and winding losses respectively. The HF transformer is built on E30x15x7 core sections made-up of N87 ferrite material using 260/42 AWG litz wire. The leakage inductance of the HF transformer referred to its primary (1.66 μH) is used as a part of resonant inductor. All the capacitors used in the

resonant tank circuit are of polypropylene type to achieve good performance.

The experimental waveforms of the converter are shown in Figs.7-11. It can be seen from Fig.7 that the converter maintained excellent input line power factor throughout the load range. The three-phase HF inverter is operated above the resonant frequency, making current flow through the resonant tank circuit (inverter output current)
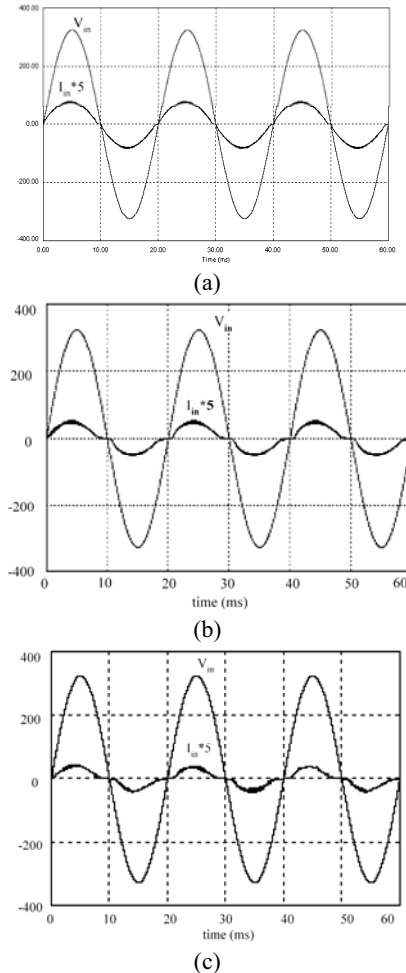

(a)

(b)

(c)

Fig. 5: PSIM simulation results of ac input voltage and input line current (a) at full load condition, (b) at 50% load and (c) at 27% load.

lagging the inverter output voltage. Hence the lagging power factor mode of operation of HF inverter is achieved. Thus, HF inverter switches turns-on only when the voltage across switches falls to zero due to already conducting their anti-parallel diodes. This results in zero-voltage switching operation of all switches. This is evident from Fig.8. The peak inverter output current and voltage across resonant capacitor went on reducing with load as it can be seen from Fig.9. Thus apart from maintaining good part load efficiency, reduced peak stresses on the resonant components were found to exist in the converter. The line-to-line voltage outputs of the three-phase HF inverter are shown in Fig.10. Fig.11 shows the experimentally obtained operating area of the HF inverter switch over one switching period at peak of ac input cycle. The operation is seen well within the safe operating area (SOA) of the device. The dc output voltage of the converter is regulated at 250 V. The output voltage and output current

waveforms of the converter at full load condition are shown in Fig.12. The overall performance of the converter is given in Table 3.
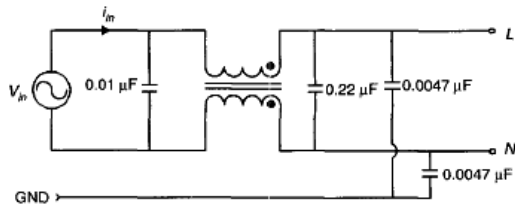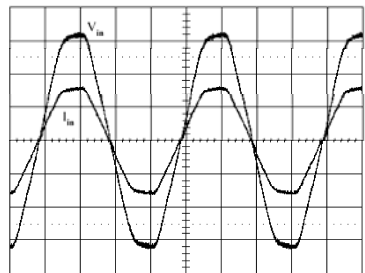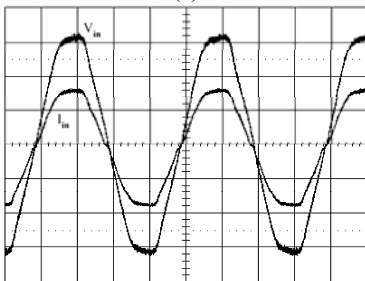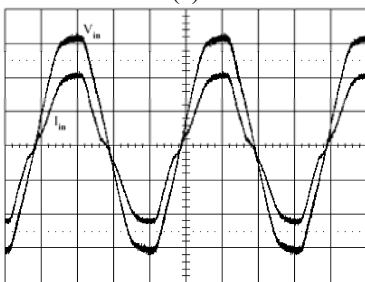

Fig.6: EMI filter at the input of ac line

(a)

(b)

(c)

Fig. 7: Experimental waveforms for input voltage and input line current for the converter under variable frequency (VF) control. Scales: time 5 mS/div, voltage 100 V/div.(a) Full load. Current scale: 10 A/div (b) 50 % load. Current scale: 5 A/div. (c) 25 % load. Current scale: 2 A/div.
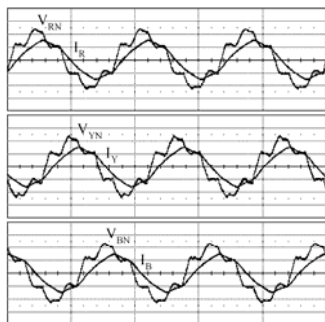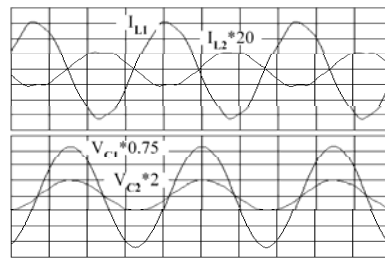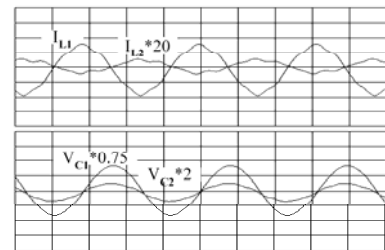
V. Conclusion

Fig. 8: Experimental waveforms for phase voltage and phase current of three-phase HF inverter under Variable frequency control at full load.. Scales: time 2 μS/div, voltage 100 V/div., Current scale: 10 A/div.

(a)

(b)

Fig. 9: Experimental waveforms for currents (I_{L1} and I_{L2}) through resonant inductors (L_1 and L_2) and capacitor voltages (V_{C1} and V_{C2}). (a) Full load, (b) 50 % load, Scales: time 1 μS/div, voltage 100 V/div, current 5 A/div.

Table 3: Overall experimental performance of the converter under variable frequency control

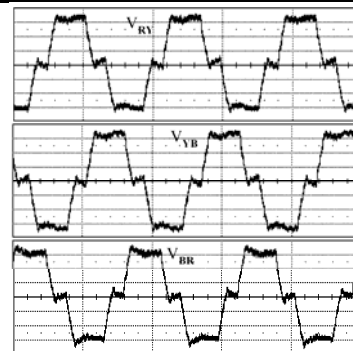| Parameter	Full load	50% Load	25% Load
Power Factor	1.00	1.00	0.99
THD (%)	3.0	3.1	7.1
Efficiency (%)	92	95	90
Switching Frequency (kHz)	290	317	370
Total HF inverter Losses, Watt	100.8	32.2	28.4
Peak Inverter current (Amp.)	16.35	8.09	4.31

Fig. 10: Experimental waveforms for line-to-line voltage output of three-phase HF inverter Scales: time 2 μS/div, voltage 100 V/div.
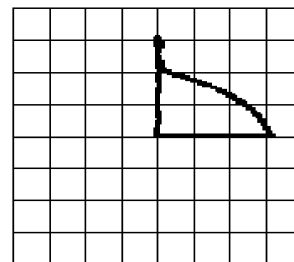

Fig. 11: Curve for the operating area of HF inverter switch over one switching period near peak of ac input cycle. Scales: voltage 100 V/div, current 5 A/div.
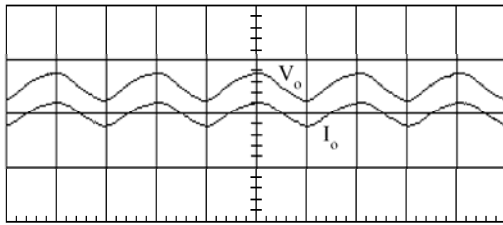
Fig. 12: Output voltage (V_0) and output current (I_0). Scales: voltage 100 V/div, current 5 A/div.

A single-phase ac-to-dc converter employing three-phase MSPRC has been proposed. This topology has several advantages such as excellent power factor without any active control of input current, usefulness for high power applications, the use of HF transformer leakage inductance as a part of resonant inductor, narrow variation of switching frequency for wider load variation, higher power packing density and minimal filtering requirements due to high switching frequency, high power conversion efficiency due to reduced conduction losses. Although the number of components required in this converter is more as compared to single-phase converter, the current and voltage stresses on these components are much lower. Such a converter will definitely be useful for high power applications.

Fourier series analysis has been carried out for the converter. The design curves for the converter have been plotted. A systematic design procedure, based on the design curves, has been given along with a design example of a 2.5 kW resonant converter. PSIM simulation and detailed experimental results have been presented. These results demonstrate the high power factor operation for the entire load range without any active control of ac input line current. The converter maintains good part load efficiency, since the peak inverter currents have been shown decreasing with the load current. The variable frequency control has been implemented for the output voltage control under varying load conditions using a digital signal processor. The converter has been shown operating in ZVS mode for the entire load range.

REFERENCES

[1] R.W.De Doncher, D.M. Divan, M.H. Kheraluwala, "A Three-Phase Soft-Switched High Power Density DC/DC Converter for High Power Applications", Industry Applications Society Annual Meeting 1988, IEEE Conference Record, Vol. 1, Oct. 1988, pp. 796-805.

[2] A.R. Prasad, P.D. Ziogas, S. Manias, "A Three-Phase Resonant PWM DC-DC Converter", Power Electronics Specialists Conference, 22nd Annual IEEE, 24-27 June 1991, pp. 463-473.

[3] W.J.B. Heffernan, P.D. Evans, M. Thompson, P. Robert, "Three Phase Parallel Loaded Resonant Converter with Fixed Frequency Operation", Fourth International Conference on Power Electronics and Variable-Speed Drives, 17-19 July 1990, pp. 115-120.

[4] A.R. Prasad, P.D. Ziogas and S. Manias, "Analysis and Design of A Three-Phase Off-Line DC-DC Converter with High-Frequency Isolation", IEEE Transactions on Industry Applications, Vol. 28, No. 4, July 1992, pp. 824-832.

[5] A.K.S. Bhat and R.L. Zheng, "A Three-Phase Series-Parallel Resonant Converter-Analysis, Design, Simulation and Experimental Results", IEEE Transactions on Industry Applications, Vol. 32, No. 4, July 1996, pp. 951-960.

[6] A.K.S. Bhat and R.L. Zheng, "Analysis and Design of A Three-Phase LCC-Type Resonant Converter", IEEE Transactions on Aerospace and Electronic Systems, Vol. 34, No. 2, April 1998, pp. 508-519.

[7] V. Pickert and C.M. Johnson, "Three-Phase Resonant Converters: An Overview", IEE Colloquium on Update on New Power Electronic Techniques, Digest No. 1997/091, 23 May 1997, pp. 2/1-2/5.

[8] S. Akre, M. Egan, M.J. Willers, "Practical Design Methodology for A New Three-Phase DC-DC Fully Resonant Converter Employing LCC-Type Tank Circuit", IEE 8th International Conference on Power Electronics and Variable-Speed Drives, 18-19 Sept. 2000, pp. 340-345.

[9] G. Drummond, "Three-Phase Resonant DC Converter for TWTs", Vaccum Electronics Conference (VEC), 27-29 April 2004, pp. 274-275.

[10] F.S. Hamdad and A.K.S. Bhat, "A Novel Soft-Switching High-Frequency Transformer Isolated Three-Phase AC-to-DC Converter with Low Harmonic Distortion", IEEE Transactions on Power Electronics, Vol. 19, No. 1, Jan 2004, pp. 35-45.

[11] M.N. Seroji and Andrew J. Forsyth, "Small-Signal Model of A High-Power-Factor, Three-Phase AC/DC Converter with Frequency Resonant Current Injection", IEEE PEDS 2005, pp. 462-467.

[12] H.M. Suryawanshi, S.G. Tarnekar, "Improvement of Power Factor Using Modified Series-Parallel Resonant Converter", IEEE Conference on Power Quality, 1998, pp. 103-109.

[13] H.M. Suryawanshi, K.L. Thakre, S.G. Tarnekar, D.P. Kothari and A.G. Kothari, "Power Factor Improvement And Close Loop Control of An AC-to-DC Resonant Converter", IEE Proceedings Electric Power Applications, Vol. 149, No. 2, March 2002, pp. 101-110.

[14] C.R. Sullivan, "Optimal Choice for Number of Strands in A Litz Wire Transformer Winding", IEEE Transactions on Power Electronics, Vol. 16, No. 2, March 2001, pp. 283-291.

[15] C.R. Sullivan, "Cost-Constrained Selection of Strand Diameter and Number in A Litz-Wire Transformer Winding", IEEE Transactions on Power Electronics, Vol. 16, No. 2, March 2001, pp. 281-288.